

Effect of pressure and temperature on the lifetime of Cr^{3+} in yttrium aluminum garnet

Y. R. Shen and K. L. Bray

Department of Chemical Engineering, University of Wisconsin, Madison, Wisconsin 53706

(Received 14 April 1997)

We have measured the room temperature (RT) and 20 K luminescence lifetime of Cr^{3+} in yttrium aluminum garnet as a function of pressure up to 240 kbar. The RT lifetime changed from 1.7(1) ms at ambient pressure to 42(2) ms at 220 kbar and the 20 K lifetime from 8.8(1) ms at ambient pressure to 67(2) ms at 240 kbar, the largest value ever observed for a Cr^{3+} -doped material. The distinct pressure dependences of the RT and 20 K lifetimes allowed us to clearly distinguish the contributions of electronic radiative decay, ${}^2E \rightarrow {}^4A_2$ vibronic transitions, and the thermal population of the 4T_2 state to the ${}^2E \rightarrow {}^4A_2$ transition of Cr^{3+} . Analysis of the temperature dependence of the ambient-pressure lifetime showed that both the ${}^2E \rightarrow {}^4A_2$ and ${}^4T_2 \rightarrow {}^4A_2$ vibronic transitions have a significant effect on the ${}^2E \rightarrow {}^4A_2$ luminescence lifetime. Within the context of the single configurational coordinate model, the coupling of the 2E and 4T_2 states via the spin-orbit coupling (\mathcal{H}_{SO}) and the electron-phonon coupling (\mathcal{H}_{EP}) mechanisms was considered in describing the observed lifetime as a function of pressure. Models formulated in either the $\mathcal{H}_{\text{EP}} > \mathcal{H}_{\text{SO}}$ or $\mathcal{H}_{\text{SO}} > \mathcal{H}_{\text{EP}}$ perturbation schemes agreed well with the lifetime data. [S0163-1829(97)02341-2]

I. INTRODUCTION

Trivalent chromium (Cr^{3+}) has been widely used as a luminescent dopant and luminescence sensitizer in various materials. Recent investigations have focused extensively on electronic structure, radiative, and nonradiative processes in octahedrally coordinated Cr^{3+} systems due to the potential application of Cr^{3+} -doped systems as tunable solid-state lasers,¹⁻³ high-temperature sensors,⁴⁻⁸ and high-pressure calibrants.^{9,10}

Spectroscopic properties of Cr^{3+} systems depend directly on the crystal-field (CF) strength (Dq/B) which determines the sequence of the two lowest excited states, the 2E doublet and 4T_2 quartet. Since the 4T_2 quartet is sensitive to Dq/B and the 2E doublet, in contrast, is insensitive to Dq/B , their energy separation, $\Delta = \mathcal{E}({}^4T_2) - \mathcal{E}({}^2E)$, varies in different Cr^{3+} systems.

The energy separation Δ has a decisive effect on the Cr^{3+} emission. When $\Delta < 0$, the low field case, Cr^{3+} luminescence occurs from the spin-allowed ${}^4T_2 \rightarrow {}^4A_2$ transition and is characterized by a broad band with a short lifetime. In the high field case, $\Delta > 0$, the Cr^{3+} luminescence arises from the spin-forbidden ${}^2E \rightarrow {}^4A_2$ transition and is characterized by sharp zero phonon R lines, phonon sideband, and relatively long lifetime. The appearance of the spin-forbidden ${}^2E \rightarrow {}^4A_2$ transition is due to a direct linkage between the spin doublet and quartet states through spin-orbit coupling. In intermediate fields, $|\Delta| \rightarrow 0$, the 2E and 4T_2 states strongly couple both thermally and through spin-orbit coupling. As a consequence, the luminescence will have characteristics of both states. Theoretical attention has been devoted to understanding the doublet-quartet coupling mechanism and recent models have been proposed to account for the effect of the 4T_2 - 2E energy separation on the emission line shape and lifetime of Cr^{3+} (Refs. 11-15).

Of particular recent interest are Cr^{3+} -based garnets. Garnet hosts are important both technologically and because

they offer an opportunity for gaining a deeper understanding of doublet-quartet mixing due to the possibility of discretely varying Δ from $\sim -1000 \text{ cm}^{-1}$ to $\sim 1000 \text{ cm}^{-1}$ in a series of isostructural crystals by varying chemical composition. Garnet crystals belong to the cubic $Ia\bar{3}d$ structure¹⁶⁻¹⁸ and have the general chemical formula $A_3B_2C_3O_{12}$, where A denotes dodecahedrally, B octahedrally, and C tetrahedrally coordinated crystallographic cation sites. Cr^{3+} ions preferentially occupy the B sites and experience an octahedral crystal field with a small trigonal distortion.^{18,19} A systematic decrease in the CF strength experienced by Cr^{3+} in garnets ($Dq/B \approx 2.59$ -2.39) was observed with increasing lattice constant in the following series: YAG ($\text{Y}_3\text{Al}_5\text{O}_{12}$)-YGG ($\text{Y}_3\text{Ga}_5\text{O}_{12}$)-GGG ($\text{Gd}_3\text{Ga}_5\text{O}_{12}$)-GSAG ($\text{Gd}_3\text{Sc}_2\text{Al}_3\text{O}_{12}$)-GSGG ($\text{Gd}_3\text{Sc}_2\text{Ga}_3\text{O}_{12}$)-LLGG ($\text{La}_3\text{Lu}_2\text{Ga}_3\text{O}_{12}$).^{11,17} More detailed analyses of the Cr^{3+} luminescence kinetics in this series of garnet crystals have attempted to describe a general theoretical coupling scheme of the 4T_2 and 2E states as a function of Dq/B or Δ .^{11-13,15,20-22}

Recent high-pressure spectroscopic studies on Cr^{3+} -doped garnets^{10,23,24} and other Cr^{3+} -activated materials²⁵⁻³⁰ have clearly demonstrated that high pressure is a powerful tool for investigating the 2E - 4T_2 coupling of Cr^{3+} systems because of its ability to continuously alter the CF strength and the 4T_2 - 2E energy separation. As a consequence, high pressure provides fine control and continuous tuning of the degree of mixing of the two coupled states of Cr^{3+} . This capability is particularly important right at the point of crossover of the 2E and 4T_2 states where their interaction is strongest and changes most abruptly with changes in Δ . Pressure is also useful, when combined with simultaneous temperature variation, for separating thermal population effects from spin-orbit coupling effects and therefore provides a finer basis for developing theoretical models. In addition, with pressure the coupling of the states can be studied in a given chemical composition thereby avoiding potential complications due to differences in factors such as defects and dopant aggregation

that may accompany changes in chemical composition.

The objective of this paper is to present combined pressure and temperature studies of Cr^{3+} in yttrium aluminum garnet (YAG). Since a pure ${}^2E \rightarrow {}^4A_2$ emission is spin-forbidden and activated via 4T_2 coupling, the lifetime of Cr^{3+} provides a quantitative reflection of the degree of 2E - 4T_2 coupling. Previous ambient pressure studies of Cr^{3+} :YAG have focused on CF analysis,³¹ absorption and excitation spectra,³²⁻³⁴ and temperature dependence of luminescence and lifetime.^{8,35-37} They provide a good basic foundation which can be expanded with high-pressure studies. A previous room-temperature (RT) study of the effect of pressure on the luminescence of Cr^{3+} :YAG up to 150 kbar¹⁰ revealed a large change in the luminescence and lifetime properties. At RT and ambient pressure, however, Cr^{3+} :YAG showed zero phonon ${}^2E \rightarrow {}^4A_2$, phonon-assisted ${}^2E \rightarrow {}^4A_2$, and broad ${}^4T_2 \rightarrow {}^4A_2$ emissions. These overlapping luminescence contributions complicate spectral analysis and hinder the theoretical analysis and understanding of the 2E - 4T_2 coupling process. In the present study, we have extended the pressure range up to 240 kbar and have considered the effect of temperature at various pressures in order to separate the different physical processes involved in the Cr^{3+} :YAG luminescence. Lifetime results as a function of pressure and temperature were quantitatively analyzed taking into account spin-orbit and electron-phonon coupling within the single configurational coordinate (SCC) model. We show that the proposed theoretical models can reasonably describe the pressure and temperature variation of the lifetime of Cr^{3+} :YAG.

II. THEORY

$\text{Cr}^{3+}(3d^3)$ ions as optical centers in a host lattice strongly interact with lattice phonons because of the spatial extent of d electrons in the solid. The coupled electron-phonon system for Cr^{3+} is described by the following vibronic Hamiltonian:^{13,38}

$$\mathcal{H} = \mathcal{H}_{\text{EL}} + \mathcal{H}_{\text{PH}} + \mathcal{H}_{\text{EP}} + \mathcal{H}_{\text{SO}}, \quad (1)$$

where \mathcal{H}_{EL} is the electronic Hamiltonian including the static crystal field potential (\mathcal{H}_{CF}), \mathcal{H}_{PH} is the lattice phonon Hamiltonian, \mathcal{H}_{EP} is the electron-phonon interaction, and \mathcal{H}_{SO} represents the spin-orbit coupling. In the Born-Oppenheimer adiabatic approximation, the vibronic wave functions can be expressed as a product of the electronic and vibrational wave functions.

A. Single configurational coordinate model

In the harmonic approximation, vibrational states are represented by harmonic oscillator wave functions, $|n\rangle$, where n is the vibrational quantum number. Using the SCC model, the vibronic wave functions for the 4T_2 quartet and 2E doublet are given by

$$\begin{aligned} |{}^2E, \alpha\rangle &= |{}^2E\rangle|\alpha\rangle, & \mathcal{E}_E^\alpha &= \mathcal{E}_E^0 + \alpha\hbar\omega, \\ |{}^4T_2, \beta\rangle &= |{}^4T_2\rangle|\beta\rangle, & \mathcal{E}_T^\beta &= \mathcal{E}_T^0 + \beta\hbar\omega, \end{aligned} \quad (2)$$

where $|\alpha\rangle$ and $|\beta\rangle$ refer to the vibrational levels of the 2E and 4T_2 harmonic electronic energy potentials. In the present

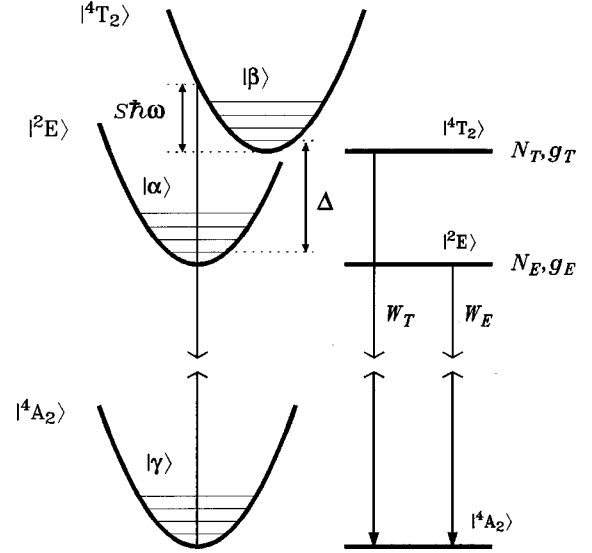


FIG. 1. Energy level diagram for Cr^{3+} :YAG. N_T and N_E are the population of the 4T_2 and 2E states. g_T and g_E denote the energy level degeneracy of the 4T_2 and 2E states, where $g_T/g_E=3$. W_E and W_T are defined as the total ${}^2E \rightarrow {}^4A_2$ and ${}^4T_2 \rightarrow {}^4A_2$ transition probabilities.

work we assume that the phonon energy $\hbar\omega$ is the same for both states. \mathcal{E}_E^0 and \mathcal{E}_T^0 are the zero phonon energies of the 2E and 4T_2 states in the absence of perturbations and are determined by the Hamiltonian $\mathcal{H}_0 = \mathcal{H}_{\text{EL}}$. Figure 1 shows the SCC diagram for the 2E and 4T_2 excited states as well as the 4A_2 ground state of Cr^{3+} (Refs. 13,15,38). The Huang-Rhys factor S measure the Franck-Condon offset for the ${}^4T_2 \leftrightarrow {}^4A_2$ transition. We have assumed no Franck-Condon offset ($S_E = 0$) for the ${}^2E \leftrightarrow {}^4A_2$ transition because the 2E and 4A_2 states belong to the same t^3 configuration.

B. 4T_2 - 2E mixing

Since it is not possible to solve the eigenvalues of Eq. (1) exactly, we have used a perturbation method. When the spin-orbit coupling is weaker than the electron-phonon interaction, $\mathcal{H}_{\text{SO}} < \mathcal{H}_{\text{EP}}$, we consider \mathcal{H}_{SO} as the perturbation. This case will be referred to as model I. If $\mathcal{H}_{\text{EP}} < \mathcal{H}_{\text{SO}}$, \mathcal{H}_{EP} is treated as the perturbation, referred to as model II. The theories have been described in detail previously in Refs. 12, 13, 15 and will only be summarized here. The summary is intended to facilitate later discussion of the experimental results.

1. Model I: $\mathcal{H}_{\text{SO}} < \mathcal{H}_{\text{EP}}$

In this model, the spin-orbit coupling is treated as a perturbation to the system. The resulting Hamiltonian becomes $\mathcal{H} = \mathcal{H}_0 + \mathcal{H}_{\text{SO}}$, where the zero-order Hamiltonian \mathcal{H}_0 contains the first three terms of Eq. (1). The energy matrix elements of \mathcal{H} based on the basis wave functions given in Eq. (2) are given by

$$\langle {}^2E, \alpha | \mathcal{H} | {}^2E, \alpha' \rangle = (\mathcal{E}_E^0 + \alpha\hbar\omega) \delta_{\alpha, \alpha'},$$

$$\langle {}^4T_2, \beta | \mathcal{H} | {}^4T_2, \beta' \rangle = (\mathcal{E}_T^0 + \beta\hbar\omega) \delta_{\beta, \beta'},$$

$$\langle {}^2E, \alpha | \mathcal{H} | {}^4T_2, \beta \rangle = \langle H_{SO} \rangle \langle \alpha | \beta \rangle, \quad (3)$$

where $\langle H_{SO} \rangle = \langle {}^2E | \mathcal{H}_{SO} | {}^4T_2 \rangle$ is the effective spin-orbit coupling constant. $\langle \alpha | \beta \rangle$ is the vibrational overlap integral and can be evaluated using Manneback recursion formulas.^{39,40} We have neglected the contribution of the spin-orbit coupling to the diagonal matrix elements because the spin-orbit coupling does not split the 2E doublet in cubic field symmetry and results in negligibly small splittings of the 4T_2 quartet.⁴¹ By diagonalizing the secular energy matrix of \mathcal{H} , we obtain the eigenvalues and the eigenvectors. The resulting perturbed 2E and 4T_2 wave functions, $|\Psi_E, m\rangle$ and $|\Psi_T, n\rangle$, are linear combinations of the basis wave functions as follows:

$$|\Psi_E, m\rangle = \sum_{\alpha} C_{E,\alpha}^m |{}^2E, \alpha\rangle + \sum_{\beta} C_{T,\beta}^m |{}^4T_2, \beta\rangle, \\ |\Psi_T, n\rangle = \sum_{\beta} C_{T,\beta}^n |{}^4T_2, \beta\rangle + \sum_{\alpha} C_{E,\alpha}^n |{}^2E, \alpha\rangle, \quad (4)$$

where the mixing coefficients $C_{E,\alpha}$ and $C_{T,\beta}$ are given by the eigenvectors. In the application of this model, a reasonably limited set of basis wave functions can be used to solve the eigenvalue problem because of the rapid convergence of the vibrational overlap integral with increasing number of vibrational quanta.

2. Model II: $\mathcal{H}_{EP} < \mathcal{H}_{SO}$

The order of the contribution of perturbations \mathcal{H}_{EP} and \mathcal{H}_{SO} has an interesting effect on the mixing between the 4T_2 quartet and the 2E doublet.¹³ The main reason for this is that \mathcal{H}_{EP} is diagonal with respect to the pure electronic 2E and 4T_2 wave functions. As a result in model I, where \mathcal{H}_{EP} is applied before \mathcal{H}_{SO} , \mathcal{H}_{EP} leads to no off-diagonal elements and does not mix the 2E and 4T_2 states. In actuality, \mathcal{H}_{EP} leads to mixing in the presence of spin-orbit coupling. Model II attempts to account for this effect by first applying \mathcal{H}_{SO} to mix the pure electronic 2E and 4T_2 . Subsequent application of \mathcal{H}_{EP} then leads to further mixing. Models I and II can therefore be viewed as different limiting case approximations of a more general model in which \mathcal{H}_{EP} and \mathcal{H}_{SO} are comparably important.

When we reverse the order of the spin-orbit and electron-phonon perturbations used in model I, we first assume the lattice is frozen at an equilibrium position. Thus, the zero-order Hamiltonian is \mathcal{H}_{EL} and the zero-order wave functions are the pure electronic states $|{}^2E\rangle$ and $|{}^4T_2\rangle$. Model II, referred to by Wojtowicz *et al.* as the frozen lattice model,¹³ includes two steps. In the first step, spin-orbit coupling is introduced as a perturbation to mix the two purely electronic states. In the second step, the electron-phonon coupling and the lattice Hamiltonian as further perturbations are included.

Spin-orbit coupling leads to mixing of the 2E and 4T_2 states and yields the following wave functions:

$$|\Phi_E\rangle = C_E |{}^2E\rangle - C_T |{}^4T_2\rangle, \\ |\Phi_T\rangle = C_T |{}^2E\rangle + C_E |{}^4T_2\rangle,$$

where

$$C_E = \sqrt{\frac{1}{2}} \left[1 + \frac{\Delta}{\sqrt{\Delta^2 + 4\langle H_{SO} \rangle^2}} \right]^{1/2}, \\ C_T = \sqrt{\frac{1}{2}} \left[1 - \frac{\Delta}{\sqrt{\Delta^2 + 4\langle H_{SO} \rangle^2}} \right]^{1/2}, \quad (5)$$

and Δ is the energy separation between the unperturbed 4T_2 and 2E states, $\Delta = \mathcal{E}_T^0 - \mathcal{E}_E^0$.

Using the spin-orbit perturbed states as basis wave functions and conventional perturbation methods, the electron-phonon interaction and the lattice Hamiltonian are then taken into account simultaneously. A rigorous solution would involve diagonalization of the resulting matrix. In the case of $\text{Cr}^{3+}:\text{YAG}$, in which a large 4T_2 - 2E energy separation is present, the off-diagonal elements are small and the following 2E vibronic wave function becomes an excellent approximation:

$$|\Psi_E, \alpha\rangle = |\Phi_E, \alpha\rangle + \sum_{\beta} \frac{\langle \beta | \mathcal{H}_{EP} | \alpha \rangle}{\Delta + \beta \hbar \omega} |\Phi_T, \beta\rangle, \quad (6)$$

where $\bar{\Delta} = \sqrt{\Delta^2 + 4\langle H_{SO} \rangle^2}$. In the assumption of linear electron-phonon coupling, the mixing coefficients can be obtained. For example, the mixing coefficient for $|\Psi_E, 0\rangle$ is given by¹³

$$C_{T,\beta}^0 = \frac{\langle \beta | \mathcal{H}_{EP} | 0 \rangle}{\bar{\Delta} + \beta \hbar \omega} = -\sqrt{2} \frac{C_E C_T}{C_E^2 - C_T^2} \\ \times \frac{-\beta \hbar \omega + \bar{S} \hbar \omega (1 - \sqrt{1/2}) \exp(-\bar{S}) \bar{S}^\beta}{\bar{\Delta} + \beta \hbar \omega} \frac{1}{\beta!},$$

where \bar{S} is defined as $\bar{S} = S(C_E^2 - C_T^2)^2$.

Models I and II, as formulated above, will be used below to describe the pressure dependence of the RT and 20 K lifetimes of $\text{Cr}^{3+}:\text{YAG}$.

III. RESULTS AND DISCUSSION

A. Experimental procedure

The sample used for the present study contains 0.5 mol % Cr^{3+} ions. Because of the large blue shift of the ${}^4T_2 \rightarrow {}^4A_2$ absorption band with pressure, different excitation wavelengths were used at low and high pressures. Below 160 kbar, pulsed 580 nm excitation obtained from a $\text{Nd}^{3+}:\text{YAG}$ laser pumped dye laser (Rhodamine 590 dye) was used. Above 160 kbar, the 532 nm pump wavelength of the $\text{Nd}^{3+}:\text{YAG}$ laser was used directly to excite Cr^{3+} . The luminescence was dispersed by a 1 m monochromator and detected by a photomultiplier tube. The luminescence decay data were collected by a 100 MHz digital storage oscilloscope capable of averaging over 1000 signal pulses. High pressure was generated in a diamond anvil cell (DAC) based on a modified Merrill-Bassett design. For low-temperature experiments, the DAC was cooled by a closed-cycle cryogenic refrigerator. The pressure was calibrated with the R_1 luminescence line of ruby.^{9,42} A 4:1 mixture of methanol-ethanol served as the pressure transmitting medium. Piermarini *et al.*⁹ showed that this mixture remains hydrostatic up to ~ 100 kbar and quasihydrostatic up to ~ 200 kbar. In the

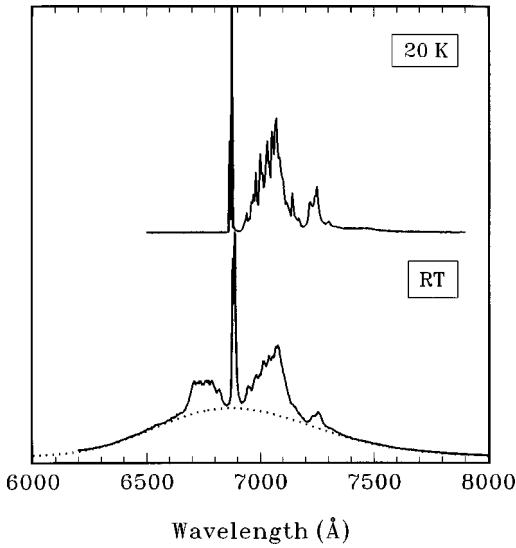


FIG. 2. Ambient pressure luminescence spectra of Cr^{3+} :YAG at 20 K and RT. The dotted curve denotes the broad ${}^4T_2 \rightarrow {}^4A_2$ emission band.

present high-pressure experiments, the well-resolved R lines and the symmetric line shapes of ruby indicated that a quasi-hydrostatic pressure distribution was maintained up to 240 kbar.

B. Ambient pressure luminescence and temperature induced R -lines shift

The luminescence features of Cr^{3+} :YAG (emission intensity, lifetime, and line position) are strongly temperature dependent.^{10,33,35,36} Figure 2 shows typical ambient pressure luminescence spectra of Cr^{3+} :YAG at RT and 20 K. The low temperature spectrum consisted of the two ${}^2E \rightarrow {}^4A_2$ zero-phonon R lines (6873.6 Å for R_1 and 6864.2 Å for R_2) and the associated Stokes phonon sideband. At RT, a structured anti-Stokes emission band appeared on the high energy side of the R lines. In addition, we observed a broad ${}^4T_2 \rightarrow {}^4A_2$ emission band (approximated with the dotted curve in Fig. 2) which develops upon thermal population of the 4T_2 state at RT.

In the temperature region 12 K–RT, the $R_{1,2}$ lines of Cr^{3+} :YAG shifted to longer wavelength with increasing temperature. The line shift as a function of temperature is shown with open circles for R_1 and open squares for R_2 in Fig. 3. The red shifts for the $R_{1,2}$ lines of Cr^{3+} :YAG with temperature from 12 K to RT were very similar, about 32 cm^{-1} , and are twice as large as the red shifts for the ruby R lines.⁴³ The temperature-induced shifts are primarily due to the coupling of optically active ions with lattice phonons and can be described by the generalized form⁴⁴

$$\Delta\mathcal{E}(T) = \alpha 2\pi \int_0^\infty \bar{D}(\omega) n(\omega) d\omega, \quad (7)$$

where $n(\omega) = [\exp(\hbar\omega/k_B T) - 1]^{-1}$, k_B is the Boltzmann constant, and α is the ion-phonon coupling constant. $\bar{D}(\omega)$ is the effective phonon density of states (DOS) resulting from the ion-phonon interaction and is related to the low-temperature vibronic structure, the phonon sideband associated with the zero-phonon line. Since the vibronic transition intensity

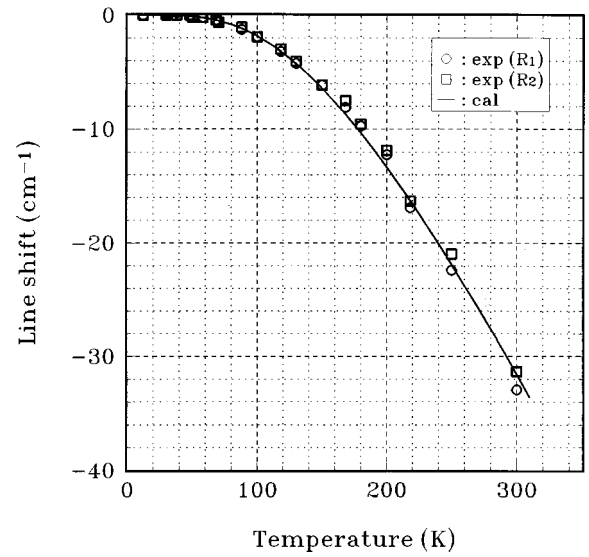


FIG. 3. Temperature dependence of the $R_{1,2}$ -lines shift of Cr^{3+} :YAG at ambient pressure.

should be proportional to both the effective phonon DOS and the probability of emitting a phonon, $1 + n(\omega)$, the effective phonon DOS for Cr^{3+} :YAG can be determined from the phonon sideband of the 20 K luminescence spectrum in Fig. 2 by a normalization procedure and is presented in Fig. 4. In the same way, the effective phonon DOS for V^{2+} :MgO was obtained by Zhang *et al.*⁴⁵ and for Sm^{2+} :KBr by Timusk and Buchanan.⁴⁶ The results for these two cases showed quite good agreement with the phonon DOS for the host crystal determined from neutron scattering experiments, referred to here as the lattice phonon DOS. Although no direct experimental data for the lattice phonon DOS of YAG crystals have been reported, the infrared spectra,^{47–49} an early Raman spectrum,⁵⁰ and our present Raman spectrum in Fig. 4 confirm that the effective phonon DOS derived from the ${}^2E \rightarrow {}^4A_2$ phonon sideband of Cr^{3+} :YAG is reasonable.

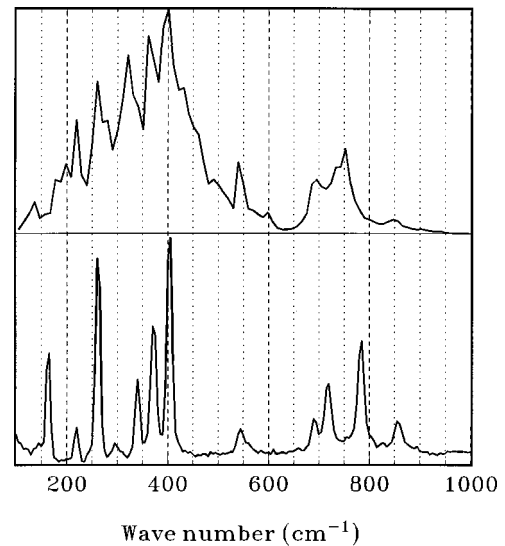


FIG. 4. Effective phonon density of states $\bar{D}(\omega)$ for Cr^{3+} :YAG (top, derived from the 20 K vibronic emission sideband shown in Fig. 2) and a room-temperature Raman spectrum of YAG upon 488 nm excitation (bottom).

When the $\bar{D}(\omega)$ of Fig. 4 is used in Eq. (7), we obtain the solid line theoretical curve for the R -line shift with temperature shown in Fig. 3. The coupling constant $\alpha = -836(40) \text{ cm}^{-1}$ was chosen to give the best fit to the line shift data and is almost twice as large as the value for ruby ($\alpha = -400 \text{ cm}^{-1}$).⁴³ It is seen from Fig. 3 that the line shift data agree well with the theoretical curve. Zhang *et al.*⁴⁵ used the effective and lattice phonon DOS to describe the temperature dependence of the linewidth and line shift in $\text{V}^{2+}:\text{MgO}$, and found that the effective phonon DOS yielded a better fit than the lattice phonon DOS. They also applied the two different phonon DOS to the specific heat for pure MgO crystal, and found that the lattice phonon DOS fits the data very well, whereas the effective phonon DOS does not. It is not surprising that the effective phonon DOS did not fit the specific heat data since the specific heat results from the phonon contribution of the entire lattice, whereas the effective phonon DOS results from only the ion-phonon interaction. On the other hand, the temperature-induced line broadening and line shift can be described very well by the effective phonon DOS because only the phonons participating in the ion-phonon interaction are important. Therefore, we believe that the effective phonon DOS obtained from the vibronic structure reasonably reflects the effect of the ion-phonon interaction on the line shift with temperature.

C. Temperature dependence of 2E lifetime

The ambient pressure 2E lifetime of $\text{Cr}^{3+}:\text{YAG}$ was measured from 12 K to RT. Figure 5 shows the present lifetime data together with those obtained by Hehir *et al.*³³ over the temperature region from 77 K to 400 K and by Fericola and Crovini⁵ from ~ 288 to ~ 550 K. These data are in close agreement with each other in the overlapping temperature regions. At temperatures below ~ 100 K, the lifetime was nearly constant. As temperature was increased above ~ 100 K, the lifetime began to decrease rapidly. This rapid decrease in lifetime with increasing temperature is mainly due to the appearance of the anti-Stokes phonon sidebands and the broad ${}^4T_2 \rightarrow {}^4A_2$ emission band, as seen from the typical RT spectrum in Fig. 2.

The temperature dependence of the 2E lifetime, under conditions of thermal equilibrium with the 4T_2 state, is given by^{22,35,38}

$$\tau_E^{-1} = \frac{W_E + W_T(g_T/g_E)\exp(-\Delta/k_B T)}{1 + (g_T/g_E)\exp(-\Delta/k_B T)}. \quad (8)$$

$$\tau_E^{-1} = \frac{W_E^0 \int_0^\infty \bar{D}(\omega) \coth(\hbar\omega/2k_B T) d\omega + W_T^0(g_T/g_E)\exp(-\Delta/k_B T)}{1 + (g_T/g_E)\exp(-\Delta/k_B T)}, \quad (9)$$

where $\bar{D}(\omega)$ is given in Fig. 4. W_E^0 , W_T^0 , and Δ are adjustable parameters which can be determined in the least squares fitting to the experimental data presented in Fig. 5.

In calculating the temperature dependence of the 2E lifetime, the temperature dependence of the energy separation Δ between the 4T_2 and 2E levels was further taken into account and was assumed to decrease linearly with temperature, $d\Delta/dT = -0.1 \text{ cm}^{-1}/\text{K}$, based on the shift rate of $-0.25 \text{ cm}^{-1}/\text{K}$ for 4T_2 (Ref. 22) and about $-0.15 \text{ cm}^{-1}/\text{K}$ for 2E obtained from Fig. 3. Our first fit of Eq. (9) to the temperature dependence of the 2E lifetime over the whole temperature region from 12 to 550 K produced the values for W_E^0 , W_T^0 , and Δ presented in Table I and the calculated result shown as curve 1 in Fig.

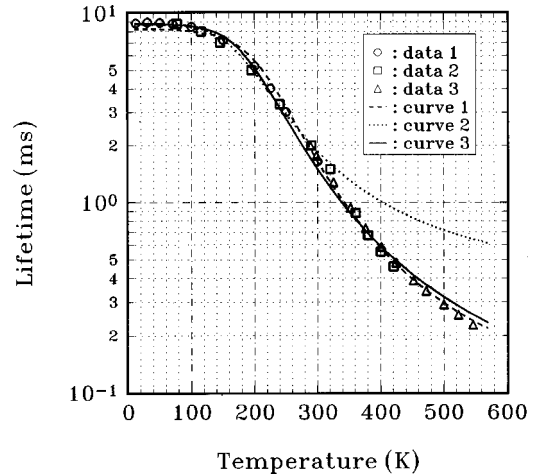


FIG. 5. Temperature dependence of the 2E luminescence lifetime of $\text{Cr}^{3+}:\text{YAG}$ at ambient pressure. Data 1: this work; data 2: Hehir *et al.* (Ref. 33); and data 3: Fericola and Crovini (Ref. 5). The curves 1, 2, and 3 were calculated using the values for W_E^0 , W_T^0 , Δ given in Table I.

When W_E and W_T in Eq. (8) are assumed to be the pure electronic radiative transition probabilities (W_E^0 and W_T^0), only the effect of the thermal population of the 4T_2 state is included in the temperature dependence of the 2E lifetime. This approach has been used previously to analyze temperature-dependent and pressure-dependent lifetime studies of Cr^{3+} in YAG and other garnets.^{10,22,35} A more complete analysis requires inclusion of the temperature dependence of the radiative decay rates of the phonon-assisted Stokes and anti-Stokes sideband transitions. The Stokes phonon process originates from emission of a phonon of energy $\hbar\omega$ with a transition probability, $\bar{D}(\omega)[1+n(\omega)]$, and the anti-Stokes phonon process originates from absorption of such a phonon with probability $\bar{D}(\omega)n(\omega)$.⁵¹ The total contribution of the two processes to the transition probability is $\bar{D}(\omega)[1+2n(\omega)] = \bar{D}(\omega)\coth(\hbar\omega/2k_B T)$. The total transition probability for the ${}^2E \rightarrow {}^4A_2$ transition of $\text{Cr}^{3+}:\text{YAG}$ may be derived by integrating over all phonon-assisted transitions: $W_E(T) = W_E^0 \int_0^\infty \bar{D}(\omega) \coth(\hbar\omega/2k_B T) d\omega$, where W_E^0 is the direct process 2E to 4A_2 transition at $T=0$ and equal to the pure electronic transition probability, W_E^0 . Thus, the temperature dependence of the τ_E lifetime can be described more fully by

TABLE I. Parameters fitted to the experimental lifetime data in Fig. 5. σ denotes the standard deviation.

Curve	Eq.	$(W_E^0)^{-1}$ (ms)	$(W_T^0)^{-1}$ (μ s)	Δ (cm^{-1})	Fitting range	σ (ms)
1	(9)	8.2(2)	43(3)	1083(21)	12–550 K	0.37
2	(9)	8.8(1)	240(20)	726(31)	12–300 K	0.22
3	(10)	8.8(1)	154(15)	828(15)	12–550 K	0.23

5. It can be noted from Fig. 5 that Eq. (9) fitted the high-temperature data closely. However, the fit over the temperature region below ~ 240 K showed a significant deviation from the data. Curve 2 represents a fit for only the data at and below RT. This restricted fit led to excellent agreement in the low-temperature region, but to a large deviation in the temperature region above RT (see curve 2 in Fig. 5).

This large deviation in the high-temperature region occurs because the broad Stokes-shifted ${}^4T_2 \rightarrow {}^4A_2$ emission is a vibronic transition with a temperature dependence that was not taken into account in Eq. (9) and that also contributes to the decrease in the 2E luminescence lifetime with increasing temperature. This effect is especially important at higher temperatures, because the broad Stokes-shifted ${}^4T_2 \rightarrow {}^4A_2$ emission becomes dominant as the thermally induced population of the 4T_2 state increases. If we incorporate the $\coth(\hbar\bar{\omega}/2k_B T)$ temperature dependence, which is valid for broad vibronic bands activated by a single odd-parity phonon mode,³⁸ for the ${}^4T_2 \rightarrow {}^4A_2$ transition, Eq. (9) becomes

$$\tau_E^{-1} = \frac{W_E^0 \int_0^\infty \bar{D}(\omega) \coth(\hbar\omega/2k_B T) d\omega + W_T^0 \coth(\hbar\bar{\omega}/2k_B T) (g_T/g_E) \exp(-\Delta/k_B T)}{1 + (g_T/g_E) \exp(-\Delta/k_B T)}, \quad (10)$$

where $\hbar\bar{\omega}$ is energy of the odd-parity phonon responsible for the vibronic process and will be assumed to be 400 cm^{-1} , the value of the most intense sideband feature shown in Fig. 4. A fit of Eq. (10) to the lifetime data in Fig. 5 using the parameters given in Table I yields curve 3. A substantial improvement in the analysis of the fit is obtained when the temperature dependence of the ${}^4T_2 \rightarrow {}^4A_2$ transition is considered.

It should be noted that the theoretical description of the temperature dependence of the 2E luminescence lifetime of $\text{Cr}^{3+}:\text{YAG}$ is mainly controlled by two parameters, the pure radiative transition probability W_T^0 for the 4T_2 quartet and the energy separation Δ between the 4T_2 quartet and the 2E doublet. Hehir *et al.*³³ observed two ${}^4T_2 \rightarrow {}^4A_2$ zero-phonon lines, 873 and 1066 cm^{-1} relative to the R_1 line, from the excitation spectrum of $\text{Cr}^{3+}:\text{YAG}$ at 77 K. The derived Δ value using Eq. (10) is very close to those observed in the excitation spectrum. The value $(W_T^0)^{-1} = 154(15) \mu\text{s}$ obtained from Eq. (10) is also close to the reported experimental 4T_2 lifetimes of $90 \mu\text{s}$ ¹¹ and $\sim 130 \mu\text{s}$ ¹⁴ for the low-field system $\text{Cr}^{3+}:\text{LLGG}$ ($\Delta_0 = -1000 \text{ cm}^{-1}$).

D. Pressure dependence of 2E lifetime

Pressure affects the 2E lifetime in a fundamentally different way than temperature. Temperature affects the lifetime primarily through the thermal population of the 4T_2 state and enhancement of radiative vibronic transitions. The energy separation Δ is only secondarily influenced by temperature. With pressure, on the contrary, an increase in Δ is the dominant effect and the thermal population and vibronic intensity effects are secondary. As a result, variations in the strength of ${}^4T_2 \rightarrow {}^2E$ spin-orbit coupling with pressure assume primary importance.

The luminescence and lifetime of $\text{Cr}^{3+}:\text{YAG}$ at RT and 20 K were measured over a pressure range of 240 kbar. The pressure dependence of the RT and 20 K lifetimes of $\text{Cr}^{3+}:\text{YAG}$ is shown in Fig. 6. The 20 K lifetime increased from $8.8(1)$ ms at ambient pressure to $67(2)$ ms at 240 kbar, while the RT lifetime increased from $1.7(1)$ ms at ambient pressure to $42(2)$ ms at 220 kbar. Since the 2E doublet and 4T_2 quartet states can couple both thermally and through the spin-orbit interaction, the pressure-induced increase in the 2E lifetime is directly related to the decoupling of these two states. The increase in the 20 K lifetime with pressure is attributed to the decrease in the purely electronic ${}^4T_2 \rightarrow {}^2E$

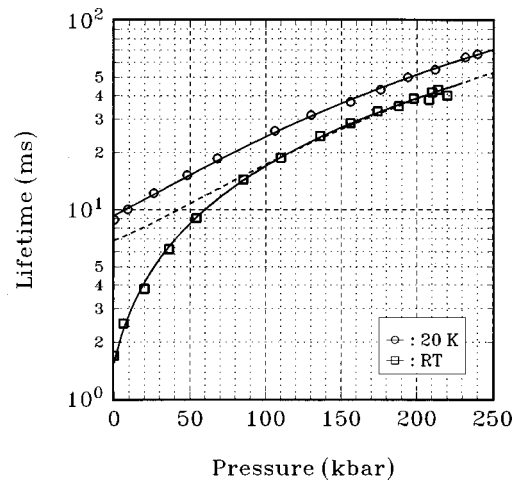


FIG. 6. Pressure dependence of the 2E luminescence lifetime of $\text{Cr}^{3+}:\text{YAG}$ at RT and 20 K. The solid lines denote polynomial fitting curves showing the trends of lifetime changes with pressure. The dashed line denotes the 20 K lifetime data multiplied by a factor of 0.71 (see text).

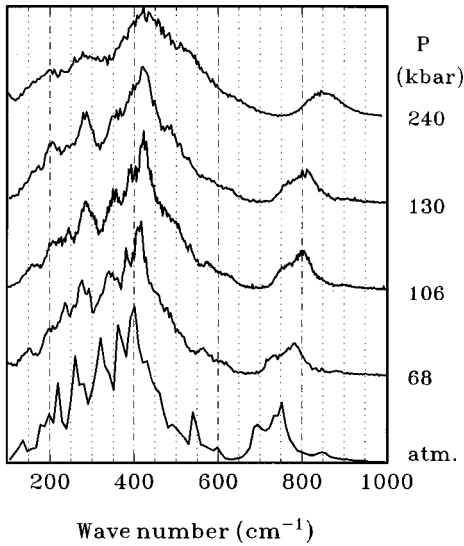


FIG. 7. Normalized ${}^2E \rightarrow {}^4A_2$ phonon sidebands of $\text{Cr}^{3+}:\text{YAG}$ at 20 K and different pressures.

admixture through the spin-orbit interaction, due to the negligible contribution of the thermal population of 4T_2 to the 2E lifetime at 20 K. Since the main effect of high pressure is to increase the 4T_2 - 2E energy separation Δ , pressure results in the reduction of the 4T_2 - 2E admixture and an increase of the 2E lifetime.

Comparing the pressure dependence of the RT lifetime with that of the 20 K lifetime, one can notice from Fig. 6 that as pressure is raised from 100 to 240 kbar, the RT and 20 K lifetimes increase keeping a constant lifetime ratio $\mathcal{R} = \tau_E(\text{RT})/\tau_E(20 \text{ K})$. The lifetime ratio is pressure independent and the value $\mathcal{R}=0.71$ was obtained from the RT and 20 K lifetime data at pressures above 100 kbar. The dashed line in Fig. 6 was obtained by multiplying the 20 K lifetime data in the entire pressure range by 0.71. The proportional difference between the 20 K and RT lifetime at pressures above 100 kbar and in the dashed line extrapolation to lower pressures is attributed to the vibronic ${}^2E \rightarrow {}^4A_2$ transition associated with the Stokes and anti-Stokes phonon sidebands. Using Eq. (10), the lifetime ratio at high pressure can be obtained if the effective phonon DOS at high pressure is known. The effective phonon DOS can be obtained from the normalized phonon sidebands and the evolution of the sidebands with pressure is shown in Fig. 7. Using the data of Fig. 7 and only the temperature-dependent vibronic 2E contribution to the lifetime in Eq. (10), we obtain $\mathcal{R}=0.69$ at ambient pressure and $\mathcal{R}=0.68$ at 240 kbar for the RT to 20 K lifetime ratio. These ratios are very close to the ratio derived directly from the experimental lifetime data, which indicates the gain in phonon sideband intensity with temperature is a reliable measure of the vibronic 2E contribution to the reduction in lifetime.

In the pressure range below 100 kbar, the thermal coupling between the 4T_2 and 2E states at RT is an additional important process. The increase in Δ with pressure results in a continuous loss and elimination of the contribution of the thermal population of the 4T_2 state to the RT lifetime. This is evident in Fig. 6, where the contribution of the thermal coupling, corresponding to the difference between the

dashed line and the measured RT lifetime, diminished with increasing pressure and was negligible above 100 kbar.

Theoretical modeling of the effects of pressure on the lifetime at RT and 20 K requires an understanding of how pressure influences the spin-orbit coupling of the 2E and 4T_2 states. The spin-orbit coupling introduces 4T_2 quartet character into the 2E doublet and relaxes spin selection rule for the ${}^2E \leftrightarrow {}^4A_2$ transition. The radiative ${}^2E \rightarrow {}^4A_2$ transition probability is proportional to the square of the mixing coefficients $C_{T\beta}$ representing components of the 4T_2 quartet in the 2E doublet. The mixing coefficients can be calculated by models I and II formulated in the previous section. Since high pressure has a large effect on the degree of mixing through variation in Δ , we expect the radiative ${}^2E \rightarrow {}^4A_2$ transition probability to be strongly dependent on pressure.

To calculate the mixing coefficients we need four physical quantities: S , $\hbar\omega$, Δ , and $\langle H_{SO} \rangle$. The Franck-Condon offset $S\hbar\omega$ can be determined from the Stokes shift, which is the energy difference between the zero phonon line and the absorption or emission maximum. The ${}^4A_2 \rightarrow {}^4T_2$ absorption band maximum in $\text{Cr}^{3+}:\text{YAG}$ occurs around 605 nm ($\sim 16500 \text{ cm}^{-1}$)^{32,52,53} and the ${}^4T_2 \rightarrow {}^4A_2$ emission band maximum is near the $R_{1,2}$ lines (see Fig. 2). Thus, the zero phonon energy of the ${}^4A_2 \leftrightarrow {}^4T_2$ transitions is estimated to be at about 15500 cm^{-1} , in close agreement with previous observed experimentally.^{33,34} These observations lead to $S\hbar\omega = \sim 1000 \text{ cm}^{-1}$ and $S = \sim 2.5$, if we use the dominant 400 cm^{-1} phonon sideband for $\hbar\omega$.

The change in Δ , the 4T_2 - 2E zero phonon energy separation with pressure can be determined from $\Delta = \Delta_0 + [d\mathcal{E}({}^4T_2)/dP - d\mathcal{E}({}^2E)/dP]P$, where Δ_0 is defined as the 4T_2 - 2E energy separation at ambient pressure. Our analysis of the temperature dependence of the ambient pressure lifetime yields $\Delta_0 = 828 \text{ cm}^{-1}$ (Table I). The shift rate $d\mathcal{E}({}^4T_2)/dP = 9 \text{ cm}^{-1}/\text{kbar}$ for $\text{Cr}^{3+}:\text{YAG}$ has previously been determined from the ${}^4T_2 \rightarrow {}^4A_2$ emission maximum up to 40 kbar. No significant change in the shape of the ${}^4T_2 \rightarrow {}^4A_2$ emission band with pressure was observed previously,¹⁰ so we assume that the band maximum and zero phonon energy change at the same rate with pressure. The ${}^2E \rightarrow {}^4A_2$ R lines were observed to shift at a rate of $d\mathcal{E}({}^2E)/dP = -0.8 \text{ cm}^{-1}/\text{kbar}$ up to 240 kbar. Combining the shift rates of the 4T_2 and 2E states gives $d\Delta/dP = \sim 10 \text{ cm}^{-1}/\text{kbar}$.

The final quantity, $\langle H_{SO} \rangle$, was the only free parameter used to calculate the mixing coefficients $C_{T\beta}$. To model the pressure dependence of the 20 K and RT lifetime data for $\text{Cr}^{3+}:\text{YAG}$ in Fig. 6, we have used Eq. (10) modified by substituting $W_T^0 \sum_{\beta} |C_{T\beta}|^2$ for W_E^0 . The spin-orbit coupling constant $\langle H_{SO} \rangle$ and the radiative 4T_2 transition probability W_T^0 were adjusted as free parameters to achieve the best fit. Within model I, 30 vibronic states for both the 2E and 4T_2 states were used to diagonalize the secular energy matrix whose elements are calculated using Eq. (3). Within model II, the 4T_2 vibronic states with contributions larger than 0.1% were taken into account in Eq. (6). Excellent agreement between the model predictions and the experimental lifetime data was obtained for $\langle H_{SO} \rangle = 211(10) \text{ cm}^{-1}$ and $(W_T^0)^{-1} = 170(10) \mu\text{s}$ within model I, and $\langle H_{SO} \rangle$

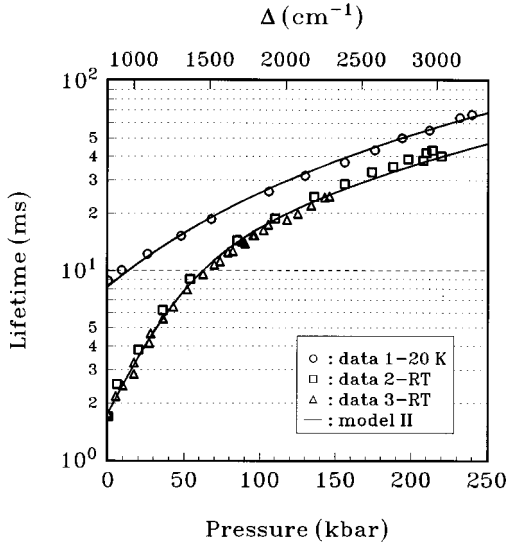


FIG. 8. Calculated and experimental results for pressure dependence of the 20 K and RT lifetimes of $\text{Cr}^{3+}:\text{YAG}$. Data 1–2 from this work and data 3 taken from Ref. 10. The solid lines denote the calculated results from model II.

$= 202(8) \text{ cm}^{-1}$ and $(W_T^0)^{-1} = 163(10) \mu\text{s}$ within model II. The calculated results from the model II are shown in Fig. 8.

The average value of $\langle H_{\text{SO}} \rangle = 207(9) \text{ cm}^{-1}$ derived from the two present models is reasonably close to the reported values of $\langle H_{\text{SO}} \rangle = 219 \text{ cm}^{-1}$ for YAG, $\langle H_{\text{SO}} \rangle = 279 \text{ cm}^{-1}$ for GGG, and $\langle H_{\text{SO}} \rangle = 319 \text{ cm}^{-1}$ for GSGG,¹⁵ as well as to the value $\langle H_{\text{SO}} \rangle = 291 \text{ cm}^{-1}$ calculated by Morrison *et al.*³¹ in a CF level simulation of $\text{Cr}^{3+}:\text{YAG}$. Struve and Huber¹¹ used the pure spin-orbit mixing model [Eq. (5)] and estimated a smaller value of $\langle H_{\text{SO}} \rangle = 105 \text{ cm}^{-1}$ in some Cr^{3+} -doped garnets. The smaller value is due to the neglect of the electron-phonon interaction and artificially compensates for the effect of a reduction of the electronic matrix elements through vibrational overlap integrals.

In our description of the electron-phonon interaction in the framework of the SCC model and in introducing the spin-orbit coupling as a perturbation, we assumed the Huang-Rhys factor S , the phonon energy $\hbar\omega$, and the spin-orbit coupling constant $\langle H_{\text{SO}} \rangle$ to be pressure-independent quantities. In fact, pressure induces slight changes in these parameters. For the Huang-Rhys factor, it has been reported in ruby that the S factor for the 4T_2 quartet decreases by 1.4% at 100 kbar from the ambient pressure value of 3.59.²⁶ The phonon energy should increase with pressure due to bond compression and stiffening of the lattice. In $\text{Cr}^{3+}:\text{YAG}$, a shift rate for $\hbar\omega$ of $< 0.4 \text{ cm}^{-1}/\text{kbar}$ can be estimated from the ${}^2E \rightarrow {}^4A_2$ phonon sidebands at different pressures shown in Fig. 7. For the pressure-induced variation in $\langle H_{\text{SO}} \rangle$, no reliable experimental result is available. From the symmetry restricted covalency model of the nephelauxetic effect in transition metal ions,^{54–57} we expect a decrease in $\langle H_{\text{SO}} \rangle$ of about 1% at 100 kbar. This prediction assumes that the decrease in the Racah B parameter in $\text{Cr}^{3+}:\text{YAG}$ with pressure is similar to that reported by Duclos *et al.*²⁶ for ruby.

The overall agreement between the model predictions and the data is excellent. The main simplifications contained in the

present study are the assumptions of the cubic field approximation and the two level scheme. In fact, there is a small trigonal field distortion from perfect octahedral symmetry present at the Cr^{3+} site in YAG. One can notice from a CF analysis of $\text{Cr}^{3+}:\text{YAG}$ at ambient pressure³¹ that the CF parameter ratio of B_3^4 to B_0^4 (1.26) is very close to the cubic field ratio ($\sqrt{10/7} = 1.20$). Furthermore, a pressure-induced decrease in the $R_{1,2}$ -lines separation was observed in previous work¹⁰ and in the present study. The 2E splitting was reduced from 19 cm^{-1} at ambient pressure to 9 cm^{-1} at 150 kbar. As pressure was increased above 150 kbar, the $R_{1,2}$ lines were unresolved due to the $R_{1,2}$ -line overlapping and the line broadening, however, the 2E splitting was estimated to be $\sim 6 \text{ cm}^{-1}$ at maximum pressure on the basis of a line shape deconvolution. Since there is negligible contribution of the spin-orbit coupling to the variation of the 2E splitting with pressure, we conclude that the observed decrease in the 2E splitting is due mainly to a pressure-induced reduction in the magnitude of the second-order trigonal field parameter B_0^2 . This indicates that the trigonal field distortion of the Cr^{3+} site in YAG decreases with increasing pressure and suggests that the cubic field approximation used in $\text{Cr}^{3+}:\text{YAG}$ at ambient pressure and high pressure is reasonable.

Finally, the two level scheme presented in Fig. 1 should be sufficient enough to allow an accurate quantitative description of the temperature and pressure dependence of the 2E lifetime in $\text{Cr}^{3+}:\text{YAG}$. Grinberg¹⁵ used an extended level scheme to describe the temperature dependence of the luminescence lifetime of Cr^{3+} in some high and intermediate field garnets. The extended level scheme was built by using seven CF energy levels, $\Gamma_8({}^2E)$, $\Gamma_8({}^2T_1)$, $\Gamma_6({}^2T_1)$, $\Gamma_6({}^4T_2)$, $\Gamma_7({}^4T_2)$, $\Gamma_8({}^4T_2)$, and $\Gamma_8'({}^4T_2)$. It was found that the seven level scheme and the two level scheme gave very similar results.

IV. CONCLUSIONS

Our investigation of the pressure and temperature dependence of the luminescence lifetime of $\text{Cr}^{3+}:\text{YAG}$ results in the following conclusions.

(1) Combined pressure and temperature studies are a powerful tool for resolving the different physical processes that govern the properties of optical materials. In the present work, we demonstrated that pressure can be used to resolve and separately quantify thermally sensitive contribution of the 4T_2 state population and vibronic transitions to the luminescence decay of Cr^{3+} .

(2) The luminescence and lifetime of Cr^{3+} -doped systems are strongly influenced by both spin-orbit coupling and electron-phonon coupling processes of the 2E and 4T_2 states of Cr^{3+} at ambient and high pressure.

(3) Proposed theoretical models that account for these processes in the context of the SCC model are able to reasonably describe the temperature and pressure variation of the lifetime of $\text{Cr}^{3+}:\text{YAG}$.

(4) More generally, the present results have demonstrated the unique ability of high pressure to continuously tune the

degree of mixing of coupled states in a system with a given chemical composition. This ability can be exploited in the study of other optical systems. Two such cases include the study of the 1E and 3T_2 states of d^2 transition metal ions (e.g., Cr^{4+} and Mn^{5+}) in a tetragonal field, and the study of strong $4f$ - $5d$ configuration interactions of divalent $4f^n$ lanthanide ions with a low-lying $5d$ state (e.g., Sm^{2+}). Investigations in these directions are currently in progress.

ACKNOWLEDGMENTS

We gratefully acknowledge financial support from the National Science Foundation under Grant No. DMR-9629990. K.L.B. also acknowledges financial support from the National Science Foundation Division of International Programs. We wish to express our thanks to Wilfred B. Holzapfel for providing his lab for our Raman scattering measurements.

- ¹J. C. Walling, H. P. Jenssen, R. C. Morris, E. W. O'Dell, and O. G. Petersen, *Opt. Lett.* **4**, 182 (1979).
- ²B. Struve and G. Huber, *J. Appl. Phys.* **57**, 45 (1985).
- ³*Tunable Lasers*, edited by L. F. Mollenauer and J. C. White (Springer, Berlin, Heidelberg, 1988), Chap. 9.
- ⁴K. T. V. Grattan, R. K. Selli, and A. W. Palmer, *Rev. Sci. Instrum.* **59**, 1328 (1988).
- ⁵Experimental lifetime data taken from Table 1 of Ref. 37 and obtained by V. Fericola and L. Crovini, in *Fiber Optic and Laser Sensors XI*, edited by R. P. DePaula, Proc. SPIE Vol. 2070 (SPIE, Bellingham, WA 1993), p. 472.
- ⁶V. Fericola and L. Crovini, in *A High-Temperature Digital Fiber-Optic Thermometer*, edited by B. Culshaw and J. D. C. Jones, Proc. SPIE Vol. 2360 (SPIE, Bellingham, WA, 1994), p. 211.
- ⁷Z. Y. Zhang, K. T. V. Grattan, and A. W. Palmer, Proc. SPIE **2101**, 476 (1993).
- ⁸Z. Y. Zhang, K. T. V. Grattan, A. W. Palmer, V. Fericola, and L. Crovini, *Phys. Rev. B* **51**, 2656 (1995).
- ⁹G. J. Piermarini, S. Block, J. D. Barnett, and R. A. Forman, *J. Appl. Phys.* **46**, 2774 (1975).
- ¹⁰P. R. Wamsley and K. L. Bray, *J. Lumin.* **59**, 11 (1994).
- ¹¹B. Struve and G. Huber, *Appl. Phys. B* **36**, 195 (1985).
- ¹²C. J. Donnelly, S. M. Healy, T. J. Glynn, G. F. Imbusch, and G. P. Morgan, *J. Lumin.* **42**, 119 (1988).
- ¹³A. J. Wojtowicz, M. Grinberg, and A. Lempicki, *J. Lumin.* **50**, 231 (1991).
- ¹⁴M. Yamaga, B. Henderson, and K. P. O'Donnell, *Phys. Rev. B* **46**, 3273 (1992).
- ¹⁵M. Grinberg, *J. Lumin.* **54**, 369 (1993).
- ¹⁶F. Euler and J. A. Bruce, *Acta Crystallogr.* **19**, 971 (1965).
- ¹⁷S. Geller, *Z. Kristallogr. Suppl.* **125**, 1 (1967).
- ¹⁸C. A. Morrison and R. P. Leavitt, in *Handbook on the Physics and Chemistry of Rare Earths*, edited by K. A. Gschneidner, Jr. and L. Eyring (North-Holland, Amsterdam, 1982), Vol. 5, p. 461.
- ¹⁹M. O. Henry, J. P. Larkin, and G. F. Imbusch, *Proc. R. Ir. Acad. Sect. A, Math. Astron. Phys. Sci.* **75**, 97 (1975).
- ²⁰M. Yamaga, B. Henderson, K. P. O'Donnell, C. T. Cowan, and A. Marshall, *Appl. Phys. B* **50**, 425 (1990).
- ²¹M. Yamaga, B. Henderson, K. P. O'Donnell, and G. Yue, *Appl. Phys. B* **51**, 132 (1990).
- ²²S. M. Healy, C. J. Donnelly, G. F. Imbusch, and G. P. Morgan, *J. Lumin.* **46**, 1 (1990).
- ²³D. Galanciak, P. Perlin, M. Grinberg, and A. Suchocki, *J. Lumin.* **60&61**, 223 (1994).
- ²⁴U. H mmerich and K. L. Bray, *Phys. Rev. B* **51**, 8595 (1995); **51**, 12133 (1995).
- ²⁵J. H. Eggert, K. A. Goettel, and I. F. Silvera, *Phys. Rev. B* **40**, 5724 (1989); **40**, 5733 (1989).
- ²⁶S. J. Duclos, Y. K. Vohra, and A. L. Ruoff, *Phys. Rev. B* **41**, 5372 (1990).
- ²⁷A. H. Jahren and M. B. Kruger, *J. Appl. Phys.* **71**, 1579 (1992).
- ²⁸J. F. Dolan, A. G. Rinzler, L. A. Kappers, and R. H. Bartram, *J. Phys. Chem. Solids* **53**, 905 (1992).
- ²⁹A. G. Rinzler, J. F. Dolan, L. A. Kappers, D. S. Hamilton, and R. H. Bartram, *J. Phys. Chem. Solids* **54**, 89 (1993).
- ³⁰P. T. C. Freire, O. Pilla, and V. Lemos, *Phys. Rev. B* **49**, 9232 (1994).
- ³¹C. A. Morrison, J. B. Gruber, and M. E. Hills, *Chem. Phys.* **154**, 437 (1991).
- ³²D. L. Wood, J. Ferguson, K. Knox, and J. F. Dillon, *J. Chem. Phys.* **39**, 890 (1963).
- ³³J. P. Hehir, M. O. Henry, J. P. Larkin, and G. F. Imbusch, *J. Phys. C* **53**, 2241 (1974).
- ³⁴W. Nie, A. Monteil, and G. Boulon, *Opt. Quantum Electron.* **22**, S227 (1990).
- ³⁵W. A. Wall, J. T. Karpick, and B. Di Bartolo, *J. Phys. C* **4**, 3258 (1971).
- ³⁶I. N. Douglas, *Phys. Status Solidi A* **9**, 635 (1972).
- ³⁷Z. Y. Zhang and K. T. V. Grattan, *J. Lumin.* **62**, 263 (1994).
- ³⁸B. Henderson and G. F. Imbusch, *Optical Spectroscopy of Inorganic Solids* (Oxford Science, New York, 1989).
- ³⁹C. Manneback, *Physica (Amsterdam)* **17**, 1001 (1951).
- ⁴⁰C. W. Struck and W. H. Fonger, *Understanding Luminescence Spectra and Efficiency Using W_p and Related Functions* (Springer-Verlag, Berlin, 1991).
- ⁴¹Since spin-orbit coupling splits the 4T_2 quartet into one Γ_6 , one Γ_7 , and two Γ_8 levels in cubic field symmetry and does not mix states from the different irreducible representations, only the Γ_8 components of the 2E doublet and the 4T_2 quartet should be taken into account. Neglecting the spin-orbit splittings of 4T_2 , one can obtain $\langle H_{SO} \rangle \approx \sqrt{4/3}\zeta$, where ζ is the spin-orbit coupling coefficient, discussed in detail by Grinberg (Ref. 15).
- ⁴²R. A. Noack and W. B. Holzapfel, in *High Pressure Science and Technology*, edited by K. D. Timmerhaus and M. S. Barber (Plenum Press, New York, 1979), Vol. 1, p. 748.
- ⁴³D. E. McCumber and M. D. Sturge, *J. Appl. Phys.* **34**, 1682 (1963).
- ⁴⁴B. Di Bartolo, in *Disordered Solids: Structures and Processes*, edited by B. Di Bartolo (Plenum Press, New York, 1989).
- ⁴⁵X. X. Zhang, P. Hong, and B. Di Bartolo, *Solid State Commun.* **81**, 117 (1992).
- ⁴⁶T. Timusk and M. Buchanan, *Phys. Rev.* **164**, 345 (1967).
- ⁴⁷G. A. Slack, D. W. Oliver, R. M. Chrenko, and S. Roberts, *Phys. Rev.* **177**, 1308 (1969).

- ⁴⁸A. M. Hofmeister and K. R. Campbell, *J. Appl. Phys.* **72**, 638 (1992).
- ⁴⁹R. Lu, K. D. Jackson, and A. M. Hofmeister, *Can. Mineralogist* **31**, 381 (1993).
- ⁵⁰J. A. Koningstein and O. S. Mortensen, *J. Mol. Spectrosc.* **27**, 343 (1968).
- ⁵¹G. F. Imbusch, W. M. Yen, A. L. Schawlow, D. E. McCumber, and M. D. Sturge, *Phys. Rev.* **133**, A1029 (1968).
- ⁵²W. Nie and G. Boulon, *Chem. Phys. Lett.* **160**, 597 (1989).
- ⁵³G. Armagan, B. Di Bartolo, and A. M. Buoncristian, *J. Lumin.* **44**, 129 (1989).
- ⁵⁴C. K. Jørgensen, *Orbitals in Atoms and Molecules* (Academic Press, New York, 1962).
- ⁵⁵D. J. Newman, Betty Ng, and Y. M. Poon, *J. Phys. C* **17**, 5577 (1984).
- ⁵⁶D. J. Newman, *Aust. J. Phys.* **30**, 315 (1978).
- ⁵⁷S. Sugano, Y. Tanabe, and H. Kamimura, *Multiplets of Transition Metal Ions in Crystals* (Academic, New York, 1970).